inorganics

MDPI

Article

Effect of Doping ZrO_2 on Structural and Thermal Properties

Mirela Petriceanu [1,2], Florentina Gabriela Ioniță [1], Radu Robert Piticescu [1], Adrian Ionuț Nicoară [1,3], Alexandru Cristian Matei [1], Miruna Adriana Ioța [1,4], Ioan Albert Tudor [1], Ștefania Caramarin [1] and Cristina Florentina Ciobota [1,*]

[1] National Institute for Non-Ferrous and Rare Metals—IMNR, 102 Biruintei Blvd., 077145 Pantelimon, Romania; mirela.petriceanu@imnr.ro (M.P.); gabriela.ionita@imnr.ro (F.G.I.); rpiticescu@imnr.ro (R.R.P.); adi.nicoara18@gmail.com (A.I.N.); alex.matei@imnr.ro (A.C.M.); iota.miruna@imnr.ro (M.A.I.); atudor@imnr.ro (I.A.T.); schiriac@imnr.ro (Ș.C.)

[2] Faculty of Biotechnical Systems Engineering, National University of Science and Technology Politehnica Bucharest, 060042 Bucharest, Romania

[3] Department of Science and Engineering of Oxide Materials and Nanomaterials, Faculty of Chemical Engineering and Biotechnologies, National University of Science and Technology Politehnica Bucharest, 060042 Bucharest, Romania

[4] Doctoral School Materials Science and Engineering, National University of Science and Technology Politehnica Bucharest, Splaiul Independentei No. 313, Sector 6, 060042 Bucharest, Romania

* Correspondence: crusti@imnr.ro; Tel.: +40-213522048

Abstract: The aim of this paper was to investigate the structure and thermal properties of zirconia ceramics co-doped with rare earth (RE) elements in equimolar concentrations. We prepared $(1 - x)ZrO_2 - x(yLa_2O_3 + yNd_2O_3 + ySm_2O_3 + yGd_2O_3 + yYb_2O_3)$ (x = 0.2; y = 0.2) powders by a hydrothermal method in mild conditions (200 °C, 2 h, 60–100 atm.) The powder was analyzed by XRD, SEM-EDAX, BET, and FT-IR after synthesis and heat treatments at 1200 °C and 1500 °C. The samples exhibit good thermal stability, with a single cubic phase presented after heat treatment at 1500 °C. The compound exhibits a low thermal conductivity (0.61 $W \cdot m^{-1} \cdot K^{-1}$), a low heat capacity (0.42 $J \cdot g^{-1} K^{-1}$), and a low thermal diffusivity (0.34 $mm^2 \cdot s^{-1}$). The values are lower than reported for conventional RE-doped zirconia.

Keywords: rare earth zirconate RE-ZrO_2; structural properties; thermal stability; thermal conductivity

check for updates

Citation: Petriceanu, M.; Ioniță, F.G.; Piticescu, R.R.; Nicoară, A.I.; Matei, A.C.; Ioța, M.A.; Tudor, I.A.; Caramarin, Ș.; Ciobota, C.F. Effect of Doping ZrO_2 on Structural and Thermal Properties. *Inorganics* **2024**, *12*, 290. https://doi.org/10.3390/inorganics12110290

Academic Editor: Chiara Dionigi

Received: 3 October 2024
Revised: 28 October 2024
Accepted: 29 October 2024
Published: 6 November 2024

1. Introduction

Ceramics based on doped zirconia may be designed to have specific functionalities; therefore, they are widely employed in a variety of sectors. Doped zirconia is a popular coating material for components like turbine blades and vanes in jet engines, power plants, and other high-temperature machinery. It provides excellent thermal insulation, protecting underlying parts from corrosion and improving engine efficiency [1].

Zirconium dioxide exhibits three polymorphs depending on the temperature: monoclinic (up to 1170 °C), tetragonal (1170–2370 °C), and cubic (2370–2680 °C). Because of the unique features of these phases, ZrO_2-based materials can be used in a wide range of applications [2]. Phase control by stabilization is necessary to achieve the desired properties regarding ZrO_2. By doping zirconia with oxides of lower-valency cations, tetragonal and cubic polymorphs of zirconia can be stabilized at room temperature [3]. The cubic phase is the most stable zirconia phase at high temperatures [4]. By stabilizing this phase through rare earth doping, the material resists detrimental phase transformations (such as tetragonal to monoclinic) that can occur at lower temperatures. These transformations can lead to microstructural changes, cracking, and reduced mechanical properties [5].

The doping of ZrO_2 with RE elements is a rapidly developing field, and new applications for these materials are being discovered all the time. Because of their exceptional

qualities, including high-temperature phase stability, low thermal conductivity, high melting points, and molten salt corrosion resistance, rare earth zirconates (RE-ZrO_2, RE = La, Gd, Sm, Yb, Nd, etc.) have been the most promising coating material for more than ten years [6–9].

The addition of RE (La, Sm, Gd, Yb, Nd) dopants to ZrO_2 can improve its properties in a number of ways: (i) It can stabilize the cubic phase of ZrO_2, which is more desirable than the monoclinic phase because it is stronger and more resistant to crack propagation [10]. (ii) It can increase the ionic conductivity of ZrO_2, which makes it more suitable for use in solid oxide fuel cells (SOFCs) [11]. (iii) It can improve the thermal conductivity of ZrO_2, which makes it more resistant to thermal shock, corrosion [12]. (iv) It can reduce the dielectric constant of ZrO_2, which makes it more suitable for use in capacitors [13].

Rare earth impurities generally cause complex changes to the diffusion coefficients, crystallographic anisotropy, and interfacial energies. Consequently, the porosity, particle-size distribution, and sintering resistance are all affected by the processing preparation technique and dopant element used. Clearly, comprehensive research using a variety of techniques is needed to fully comprehend these phenomena [14].

The cubic phase of rare earth doped ZrO_2 greatly improves its high-temperature resistance. The cubic phase of zirconia is the most stable at high temperatures [15]. Furthermore, the thermal expansion coefficient of the cubic phase frequently equals that of other materials utilized in high-temperature applications. This matching lowers thermal stresses and the risk of cracking or delamination during thermal cycling.

Trivalent dopants (La, Sm, Gd, Nd, Yb) cause structural deformation and the development of oxygen vacancies, successfully stabilizing the tetragonal and cubic structure of ZrO_2. As a result, it is anticipated that large-ion trivalent elements will successfully stabilize ZrO_2's structure. La, in particular, has garnered interest as a possible stabilizer of ZrO_2's structure due to its large ionic radius and low oxygen vacancy formation energy [16].

Until now, numerous methods, including combustion [17], precipitation, and sonochemical [18] and hydrothermal [19] processes, have been applied to fabricate zirconia. Hydrothermal technology is accessible, efficient, and environmentally friendly [20]. The benefits of hydrothermal methods over other synthesis processes include its ability to obtain crystalline materials quickly, the lack of ulterior thermal treatments, and its independent control over parameters, including concentration, temperature, and pressure. This is shown in Table 1 [19].

Table 1. Advantages and disadvantages of hydrothermal methods.

Hydrothermal Process	
Advantages	**Disadvantages**
It is possible to control the size, shape, and morphology of the materials.	The method can be complex, requiring careful control of various parameters.
Low environmental impact	The autoclaves can be expensive.
Versatility (metal oxide, doped oxides, organic/inorganic structures)	Hydrothermal reactions can sometimes take a long time, impacting efficiency.
High-quality powders	The reaction takes place in a closed system, making it impossible to see firsthand.
Large-scale production	Working conditions can lead to reactor corrosion.
Refs. [21,22]	Refs. [21,23]

The aim of this paper is to investigate the influence of doping elements on the structural and thermal properties of a nanostructured doped ZrO_2 material, synthesized by the hydrothermal method, as an anticorrosive material. We determined its physical properties and thermal behavior.

2. Results and Discussion

Chemical, morphological, structural, and thermal conductivity analyses were performed to better understand the behavior of the nanostructured powder of ZrO_2-LSGYN. The results are presented below.

2.1. Chemical Composition of ZrO_2-LSGYN

The ZrO_2-LSGYN sample, as obtained after the hydrothermal process, was characterized from the point of view of chemical composition; the presence of Zr, La, Sm, Gd, Yb, and Nd was determined by ICP-OES. Theoretical molar formula of the sample was as follows: $(1 - x)ZrO_2\ x(yLa_2O_3 + yNd_2O_3 + ySm_2O_3 + yGd_2O_3 + yYb_2O_3)$. In this formula, x = 0.2 and y = 0.2. This analysis was not performed on the heat-treated samples because we did not consider it necessary as the concentration elements would not change with temperature. Spectroscopy was carried out according to [24] ASTM E1479-24. The results of the elemental analysis are presented in Table 2.

Table 2. The results of the elemental analysis as determined by ICP-OES.

Chemical Analysis wt.%					
Zr	**La**	**Sm**	**Gd**	**Yb**	**Nd**
41.8	7.44	6.60	7.85	8.74	6.32

2.2. X-Ray Analysis of ZrO_2-LSGYN Samples

Pure ZrO_2 exists in three polymorphs: the monoclinic phase (space group C52h or P21/c) is stable at low temperatures. The phase transition to a tetragonal structure (space group D154h or P42/nmc) occurs at around 1127 °C. The tetragonal phase changes into one with a cubic fluorite structure (space group O5h or Fm3m) at roughly 2327 °C. This structure then melts at 2677 °C [25].

Over a broad temperature range, zirconia's tetragonal and cubic phases can be stabilized by a small amount of rare earth solutes [14].

As illustrated in Figure 1, the thermally untreated sample has a phase configuration composed of a mixture of crystalline phases consisting of components with tetragonal P42/nm symmetry, (identified by ICDD 04-014-2971), monoclinic P21/c symmetry (identified by ICDD 04-010-3278), and cubic I3-3m symmetry. This was identified by ICDD 04-007-2358. For this sample, the crystallinity degree obtained by Rietveld analyses was 41.8%. The ultrafine nanoparticles are indicated by the wide peak broadenings of the as-synthetized sample; the degree of crystallinity increases and the peak widths become narrower with increasing temperature [26].

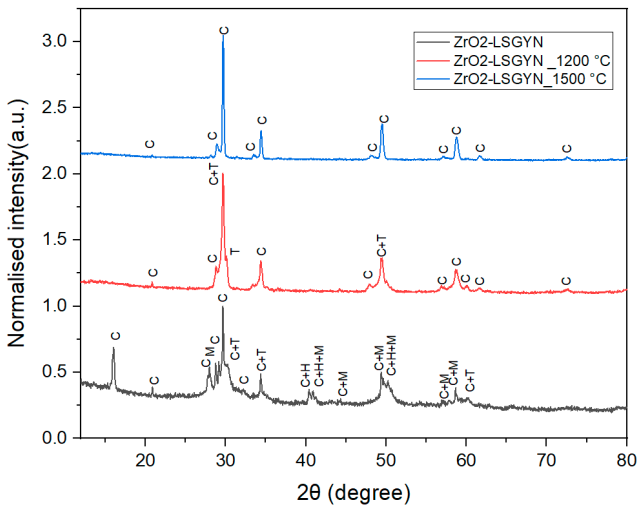

Figure 1. X-ray diffractograms of ZrO_2-LSGYN.

As the sintering temperature increases to 1200 °C, the crystallinity degree of the samples increases up to 52.41%; the phase mixture consists of a ZrO_2 cubic Fm-23m symmetry phase (identified by ICDD 04-005-9865) and a tetragonal P42/nmc symmetry phase. At sintering temperatures of 1500 °C, only the presence of the cubic phase could be determined and the crystallinity degree exceeded 58.97%. The Rietveld refinement (see Figure 2) of the obtained diffractograms had optimal agreement parameters for the assignment of cubic phases (sample ZrO_2-LSGYN_1500) of R_{xp} = 5.44054, R_p = 4.16748 R_{wp} = 5.9777, respectively, goodness of fit (χ^2) = 1.20, thus ensuring the accuracy of the assignment.

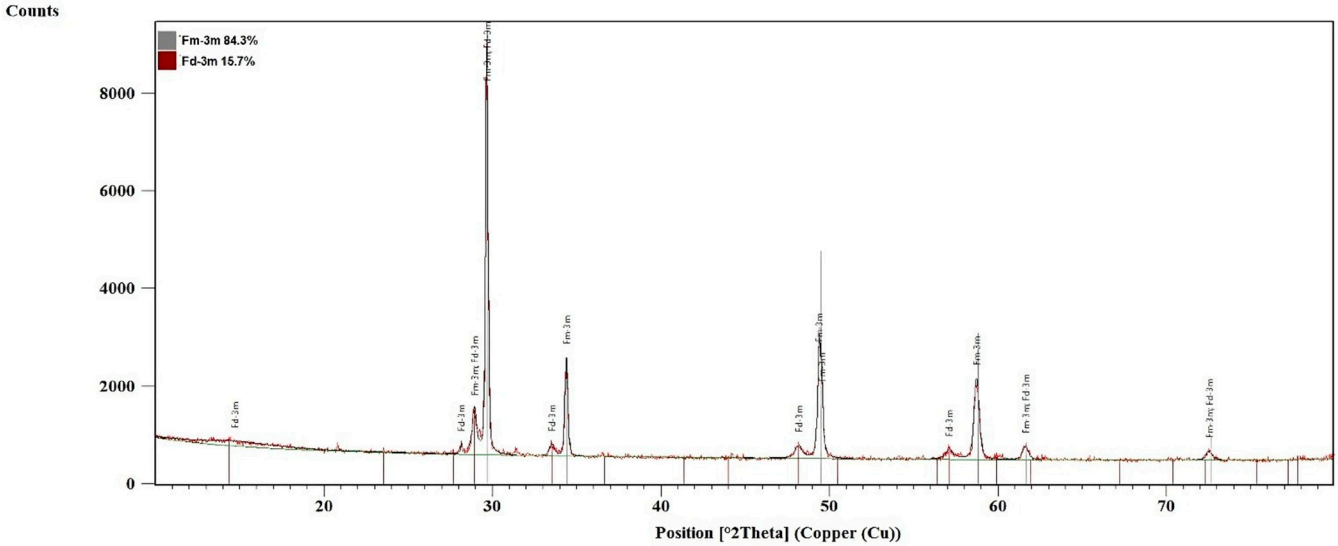

Figure 2. Rietveld refinement for ZrO_2-LSGYN_1500 (relevant for other sample as well).

Figure 1 shows the X-ray diffraction patterns recorded at room temperature for ZrO_2-LSGYN samples obtained at different temperatures, while Table 3 shows the unit cell parameters obtained after Rietveld refinement of the experimental data.

Table 3. The cell parameters obtained by Rietveld refinement.

	ZrO_2-LSGYN			**ZrO_2-LSGYN_1200**		**ZrO_2-LSGYN_1500**
ICDD PDF4+	04-014-2971	04-010-3278	04-007-2358	04-005-9865	00-024-1164	04-005-9865
Symmetry	P42/nmc	P21/c	I3-3m	Fm-3m	P42/nmc	Fm-3m
a [Å]	3.63293	5.12066	4.43861	5.21287	3.60927	5.2088
b [Å]	3.63293	5.26207	4.43861	5.21287	3.60927	5.2088
c [Å]	5.22511	5.43056	4.43861	5.21287	5.19192	5.2088
alpha [°]	90	90	90	90	90	90
beta [°]	90	99.68192	90	90	90	90
gamma [°]	90	90	90	90	90	90
Volume [$Å^3$]	68.96	144.2437	87.44632	141.6545	67.63442	141.3234
Crystal system	Tetragonal	Monoclinic	Cubic	Cubic	Tetragonal	Cubic
R_{wp}		6.3733		4.8630		5.9777

2.3. BET Surface Analysis of ZrO_2-LSGYN

For each sample, a Brunauer–Emmett–Teller (BET) surface area analysis was performed in order to determine physical characteristics such as surface area and porosity. The surface area was calculated to be 140.76, 6.89, and 0.49 m^2 /g for ZrO_2-LSGYN,

ZrO_2-LSGYN_1200, and ZrO_2-LSGYN_1500 respectively. The Barrett−Joyner−Halenda (BJH) average pore size was found to be 7.99 nm for ZrO_2-LSGYN, 6.88 nm for ZrO_2-LSGYN_1200, and 4.98 nm for ZrO_2-LSGYN_1500 (Figure 3). The average pore size range indicates that the material is mesoporous, which matches the results of the SEM analysis. N_2-adsorption−desorption isotherm plots indicate a type IV category for ZrO_2-LSGYN. For ZrO_2-LSGYN_1200 and ZrO_2-LSGYN_1500, the isotherms are type III according to IUPAC references, due to capillary condensation on the surface of mesoporous materials [27–29].

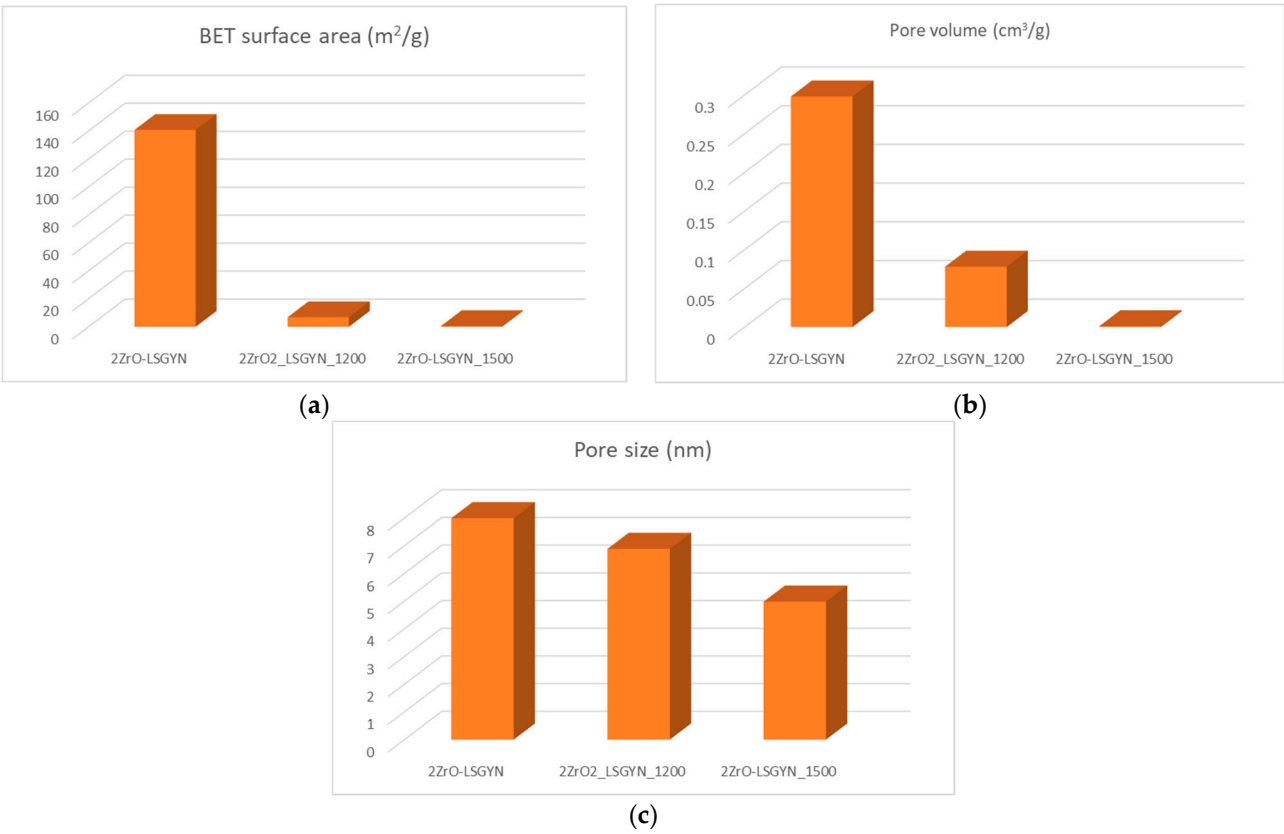

Figure 3. BET surface area analysis results: plots for (**a**) BET surface area, (**b**) pore volume, and (**c**) pore size.

The ZrO_2-LSGYN sample calcined at 1500 °C shows lower adsorption over the entire pressure range compared to the ZrO_2-LSGYN_1200 and ZrO_2-LSGYN samples (Figure 4). This correlates with the decrease in pore volume in the case of the sample calcined at 1200 °C and 1500 °C.

The particle-size study highlights the formation of nanostructured powders. This demonstrates that nanometric particles were formed under hydrothermal conditions, with particle sizes of 7.50 nm for ZrO_2-LSGYN, 153.26 nm for ZrO_2-LSGYN_1200, and 2074.16 nm for ZrO_2-LSGYN_1500.

At high temperatures, increased atomic mobility within the material allows adjacent particles to fuse together, reducing pore volume and shrinking existing pores; this effect is more pronounced in nanostructured materials. This densification process is particularly pronounced in these doped zirconia materials due to their lower melting points and ionic radius differences. Compared to pure ZrO_2, the incorporation of these dopant elements often lowers the overall melting point of the material. This increased susceptibility to thermal activation at lower temperatures facilitates sintering at a faster rate. Also, the dopant elements (La, Sm, Gd, Yb, Nd) have larger ionic radii compared to Zr^{4+}. This size difference can introduce lattice distortions and oxygen vacancies within the crystal

structure, creating additional diffusion pathways for atoms and further accelerating the sintering process [30,31].

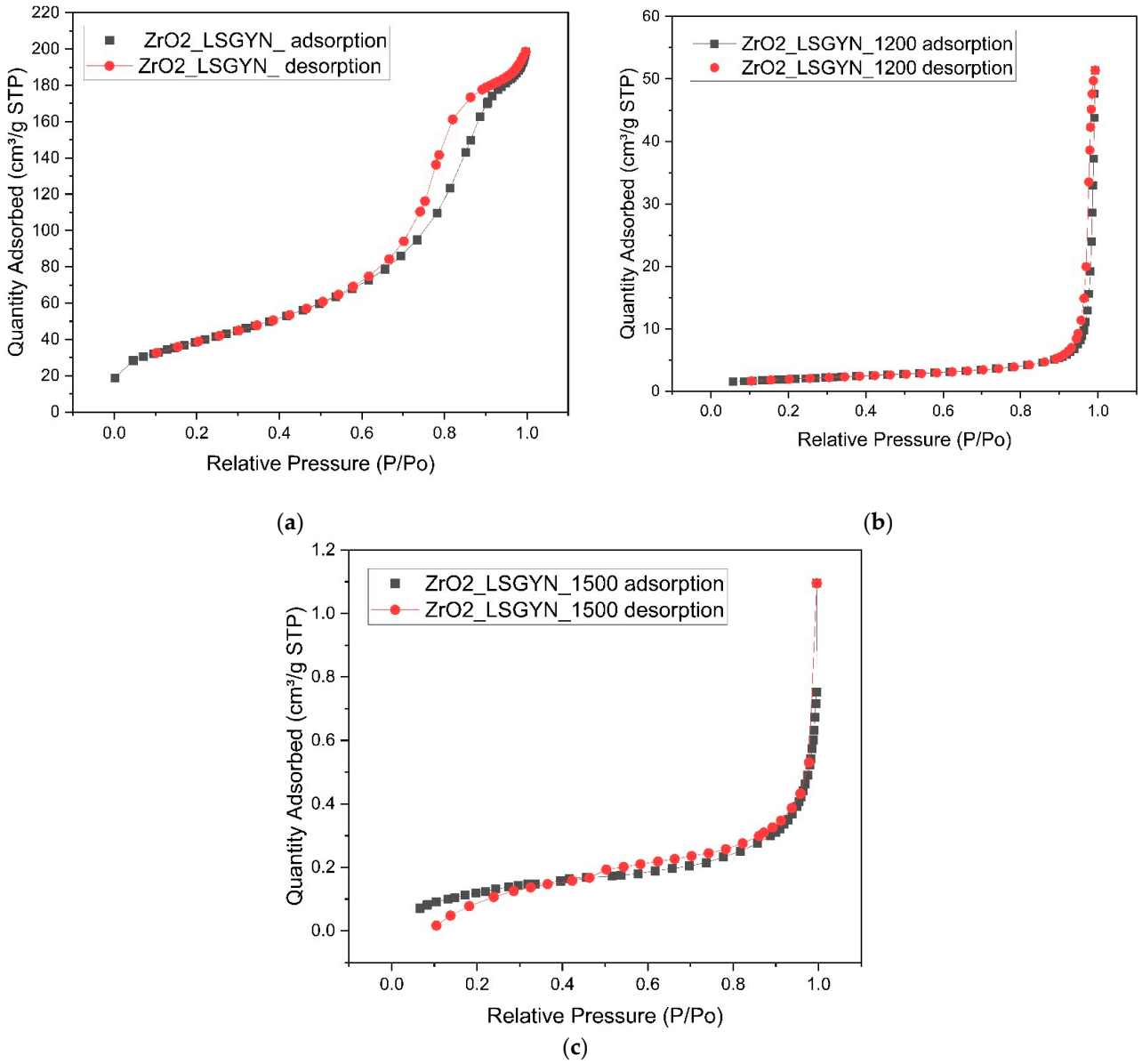

Figure 4. BET surface area analysis results: N_2-adsorption−desorption isotherm plots. (**a**) ZrO_2-LSGYN as synthetized; (**b**) ZrO_2-LSGYN heat-treated at 1200 °C; (**c**) ZrO_2-LSGYN heat-treated at 1500 °C.

2.4. Scanning Electron Microscopy Analysis of ZrO_2-LSGYN

The morphologies of the ZrO_2-LSGYN, and of the heat-treated samples at 1200 °C and 1500 °C are shown in Figure 5. The particles in the synthesized sample appear to be agglomerated, resembling irregularly shaped formations. At 1200 °C the samples tend to present a rounded particle shape, and at 1500 °C the powder starts to form large aggregate (10 µm). We compared the data weight concentrations from chemical analysis and from EDS analysis of the ZrO_2-LSGYN sample. Table 4 presents a comparison between EDS and chemical elemental weight percentage values for the sample that was not heat-treated. As can be observed, the results for the Zr, La, Sm, Gd, Nd, and Yb elements are comparable.

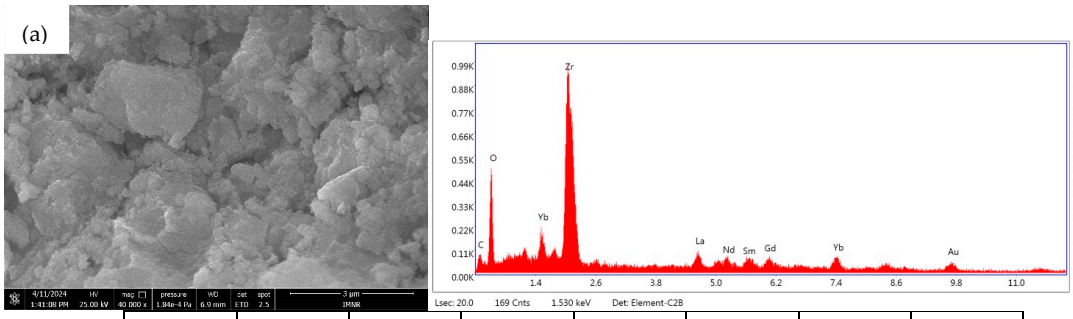

Element	Weight %	Atomic %	Net Int.	Error %	P/B Ratio	R	F
ZrL	40.20	35.81	436.29	10.24	179.4019	1.0343	1.0029
LaL	6.39	3.74	44.65	24.45	30.1937	1.0671	1.0170
NdL	4.51	2.54	28.93	29.30	21.4111	1.0718	1.0198
SmL	4.43	2.39	25.43	32.05	20.5120	1.0748	1.0228
GdL	5.31	2.75	27.01	39.67	23.7267	1.0776	1.0250
YbL	12.37	5.81	43.69	24.04	48.3124	1.0857	1.0305

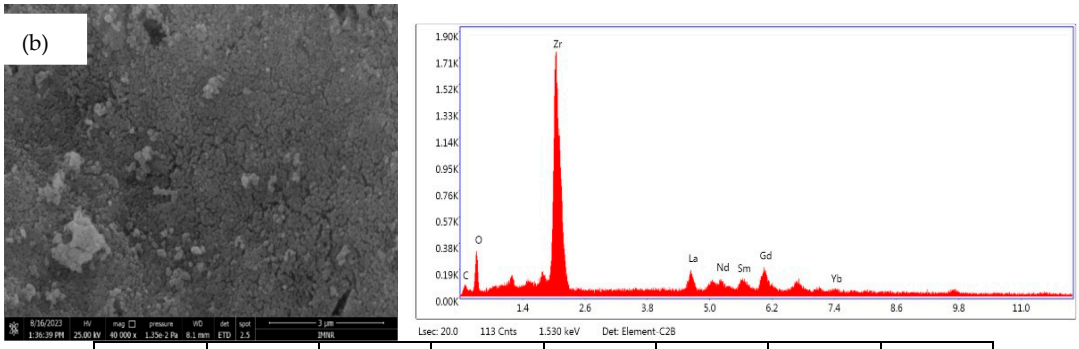

Element	Weight %	Atomic %	Net Int.	Error %	P/B Ratio	R	F
ZrL	64.36	58.77	840.60	8.99	236.5311	1.0227	1.0028
LaL	7.95	4.77	82.56	16.72	34.9245	1.0521	1.0163
NdL	4.39	2.54	45.57	25.20	19.8744	1.0562	1.0164
SmL	5.27	2.92	50.77	22.89	23.7352	1.0589	1.0184
GdL	10.52	5.57	101.99	16.89	46.5303	1.0615	1.0195
YbL	2.89	1.39	12.36	54.76	12.0838	1.0687	1.0293

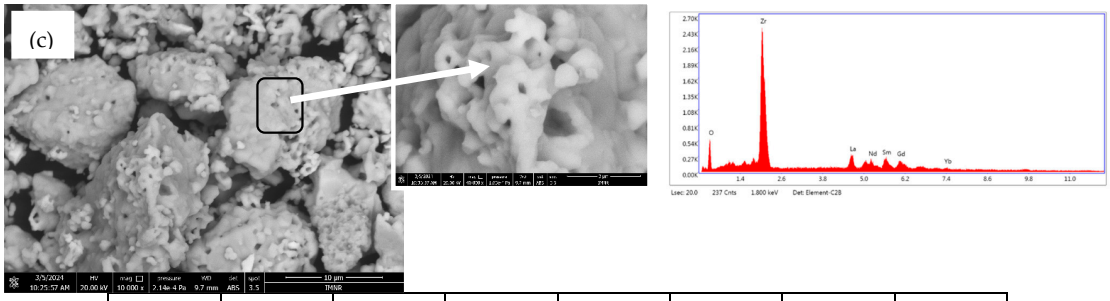

Element	Weight %	Atomic %	Net Int.	Error %	P/B Ratio	R	F
ZrL	56.91	53.71	1128.91	7.11	221.5316	1.0314	1.0029
LaL	11.97	7.42	160.61	12.86	50.4918	1.0614	1.0154
NdL	6.57	3.92	84.76	19.97	27.8947	1.0657	1.0147
SmL	9.29	5.32	111.55	15.72	38.5893	1.0684	1.0157
GdL	6.76	3.70	80.90	21.68	27.1436	1.0710	1.0166
YbL	4.06	2.02	16.12	50.17	14.4205	1.0784	1.0231

Figure 5. SEM/EDAX images of (**a**) ZrO_2-LSGYN, (**b**) ZrO_2-LSGYN heat-treated at 1200 °C, and (**c**) ZrO_2-LSGYN heat-treated at 1500 °C.

Table 4. Elements wt.% determined by chemical elemental analysis and by EDS.

Analysis Type	Elements wt.%					
	Zr	**La**	**Sm**	**Gd**	**Yb**	**Nd**
Chemical	41.8	7.44	6.60	7.85	8.74	6.32
EDS	40.2	6.39	4.43	5.31	13.37	4.51

2.5. FT-IR Analysis

To evaluate the formation and quality of the samples, as shown in Figure 6, FTIR spectroscopy is employed. The stretching vibration of the –OH group of water molecules adsorbed on the surface of ZrO_2 nanoparticles is responsible for the strong absorption band detected in the region of 3300 to 3600 cm^{-1}, while the characteristic bending vibration of the –OH group of water molecules is indicated by the peak cantered at 1540 cm^{-1} [32,33]. The stretching vibration of the hydroxyl zirconium (Zr–OH) bond is evidenced by the peaks at 2344 cm^{-1} [34]. ZrO_2 phase stretching vibration is correlated with sharp peaks detected at 560 cm^{-1} [35]. This observation validates the creation of ZrO_2 as a crystalline phase. With increasing calcination temperature, the intensity of the upper absorption band diminishes, suggesting that water molecules are removed [36].

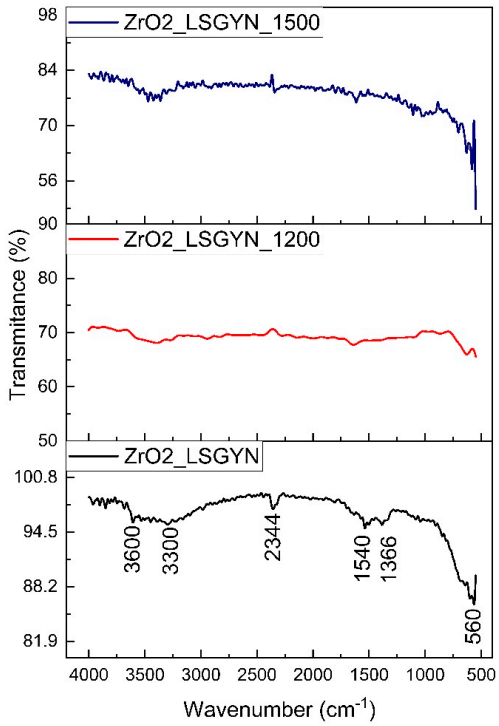

Figure 6. FT-IR spectra of ZrO_2_LSGYN as synthetized, heat-treated at 1200 °C and at 1500 °C.

2.6. DSC/TG Analysis of ZrO_2-LSGYN

Figure 7 shows the DSC-TG image of the ZrO_2-LSGYN; the mass loss of the sample is about 9.3%. The first endothermic peak between 25 and 152 °C could be associated with the water molecules of the surface (mass loss 4%) [37]. The second peak between 280 and 360 °C (mass loss 4%) may be related to the temperatures that start to promote the liberation of Cl_2 [38]. After 600 °C, there is no loss in TG curve, which may indicate the crystallization of amorphous ZrO_2 and monoclinic phase transformation. This shows that ZrO_2-LSGYN after 600 °C does not present mass loss or other transformation, agreeing with the XRD analysis; at 1200 °C, the monoclinic phase disappears, confirming the presence of the cubic and tetragonal phase [39].

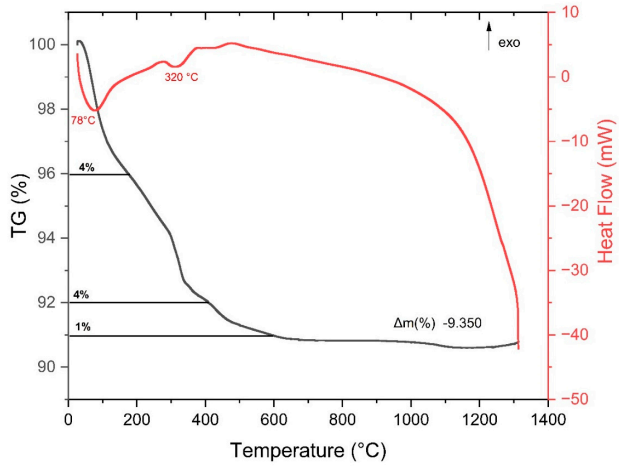

Figure 7. DSC/TG spectra of ZrO_2-LSGYN.

2.7. Thermal Conductivity

The samples used for this type of measurement were heat-treated at 1500 °C. This means, according to XRD analysis, that the cubic phase exists at this temperature.

Undoped ZrO_2 is difficult to sinter at the high densities needed for the measurement of thermal properties due to phase transitions at around 1200 °C.

The thermal conductivity of the material obtained is much lower than shown by the data provided by the literature, as can be seen in Table 5. When it comes to materials that withstand high temperatures, these ceramic materials offer a lot more promise than the most advanced partly yittria-stabilized zirconia at significantly higher temperatures. Low thermal conductivity helps to minimize temperature gradients within the ceramic coating, reducing the potential for thermal stresses that can lead to cracking and delamination.

The difference in cation radius between La^{3+}, Sm^{3+}, Gd^{3+}, Yb^{3+}, Nd^{3+}, and Zr^{4+} is significantly greater than that that between other cations like Sc^{3+} and Zr^{4+}; it makes sense that doping with more cations would result in a bigger elastic strain field. Furthermore, co-doping five oxides can result in the introduction of defect clusters [40], which can cause more severe defect dispersion and a decrease in thermal conductivity. The micromechanics of thermal conduction states that heat conduction through inorganic nonmetallic materials is caused by phonon influence [41]. The increased concentration of oxygen vacancies and substitutional defects caused by the higher overall doping amount clearly improved the phonon scattering and lessened the decrease in thermal conductivity.

The values measured in the present paper for ZrO_2-LSGYN pellets are of the same order of magnitude as those obtained in our previous paper [42], where we studied the influence of individual rare earth dopants La, Nd, Sm, and Gd on YSZ room temperature thermal conductivity using the Hot Disk method. The thermal conductivity measured was at 0.30 W/mK for YSZ-6% La, 0.32 W/mK for YSZ-6%Nd, 0.39 W/mK for YSZ-6% Sm, and 0.37 W/mK for YSZ-6%Gd.

Lower thermal diffusivity is beneficial when it comes to improved thermal shock resistance; this property also inhibits the diffusion of corrosive species (like ions or gasses) through the ceramic coating, thereby protecting the underlying substrate.

Zirconia ceramics, depending on their specific type and composition, typically have a moderate to high specific heat capacity. This ranges from around 0.470 J/g·K to 0.610 J/g·K [43]. Dopants can also influence the specific heat.

This type of material is a promising option for thermal insulation and high-temperature applications as, if these values can be extrapolated to higher temperatures, they provide attractive insulating values at room temperature.

In Table 5, we find the measurements of thermal conductivity, thermal diffusivity and volumetric specific heat, the specific heat was calculated.

Table 5. Measurements of thermal conductivity, thermal diffusivity, and volumetric specific heat, in which the specific heat was calculated.

Material	k (W/mK)	α (mm^2 /s)	Volumetric Cp (10^6 J/m^3K)	Cp (J/gK)	Ref.
ZrO_2-LSGYN	0.61 ± 0.006	0.34 ± 0.02	1.82 ± 0.11	0.42	This work
$La_2Zr_2O_7$	1.56	-	-	-	[44]
$La_{1.7}(DyNd)_{0.15}(Zr_{0.8}Ce_{0.2})_2O_7$	1.30	0.65		0.32	[41]
$La_{1.7}Dy_{0.3}Zr_2O_7$	1.65	0.75		0.37	[41]
$La_2Zr_2O_7$	1.85	0.85		0.38	[41]

3. Materials and Methods

3.1. Doped ZrO_2 Hydrothermal Synthesis

Nanostructured material $(1 - x)ZrO_2 - x(yLa_2O_3 + yNd_2O_3 + ySm_2O_3 + yGd_2O_3 + yYb_2O_3)$ (x = 0.2; y = 0.2) encoded as ZrO_2-LSGYN was synthesized in a one-step process by the hydrothermal method, starting from water-soluble salts of Zr and oxides. $ZrCl_4$ (Darmstadt, Germany, p.a. > 98%), Sm_2O_3 (Alfa Aesar, Haverhill, MA, USA, p.a. > 99.9%) Nd_2O_3 (Alfa Aesar, MA, USA, p.a. > 99.9%), Yb_2O_3 (Alfa Aesar, MA, USA, p.a. > 99.9%), Gd_2O_3 (Thermo Scientific, Waltham, MA, USA, p.a. > 99.9%), La_2O_3 (Thermo Scientific, MA, USA, p.a. > 99.9%) and NH_3 (25%) was used as mineralizers. The amounts of Sm_2O_3, La_2O_3, Nd_2O_3, Gd_2O_3, Sm_2O_3, and $ZrCl_4$ were established in agreement with the theoretical molar formula $(1 - x)ZrO_2 - x(yLa_2O_3 + yNd_2O_3 + ySm_2O_3 + yGd_2O_3 + yYb_2O_3)$ (x = 0.2; y = 0.2). The precipitation reaction pH produced a result in the range of 9.5–11. The suspension thus obtained was subjected to hydrothermal processing (pressure—100 atm; temperature—200 °C; time—2 h). The final suspension was introduced into a Teflon vessel of a sealed hydrothermal autoclave reactor (5 L, Berghof Products + Instruments GmbH, Berghof, Germany (Figure 8)) endowed with a cooling system. To control the reaction pressure, argon gas was purged inside the autoclave, according to the working procedure described in [19].

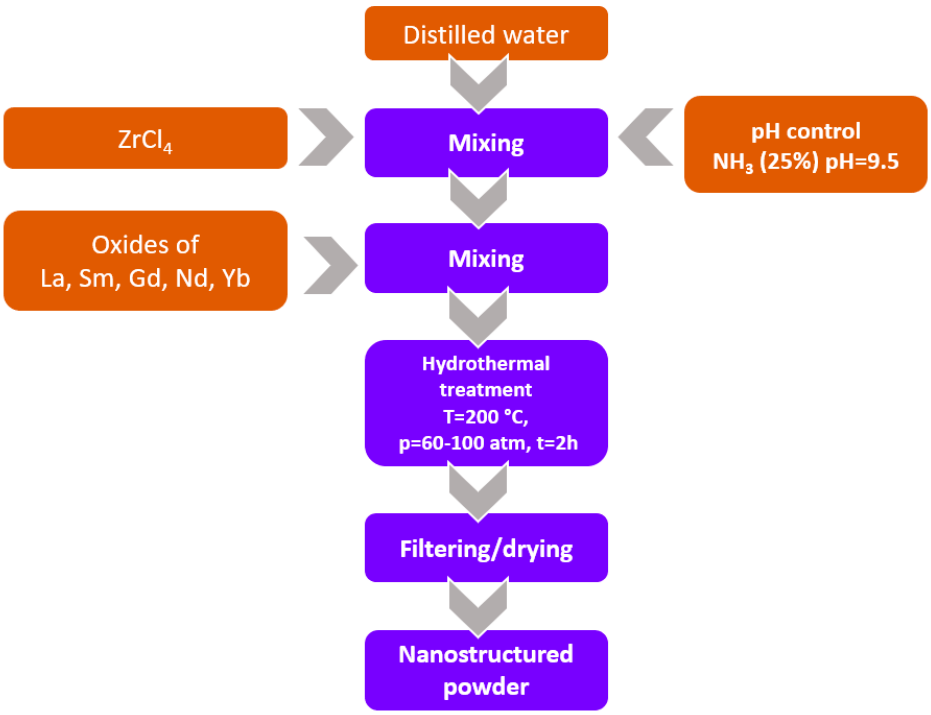

Figure 8. The schematic workflow of the synthesis.

The obtained wet precipitate was then filtered, washed with distilled water, and dried in an oven at 100 °C for 8 h. In order to study nanostructured powder behavior during thermal treatment, samples of the as-obtained ZrO_2-LSGYN were subjected to heat treatment at either 1200 °C or1500 °C for three hours, and the samples were encoded as ZrO_2-LSGYN _1200 and ZrO_2-LSGYN_1500, respectively.

3.2. Characterization

Powder was characterized from the chemical point of view via the Inductively Coupled Plasma Atomic Emission Spectroscopy (ICP-OES) technique, using ICP-OES 725 (AGILENT, Santa Clara, CA, SUA) equipment, according to the [45] ASTM E1479-16 standards.

The phase composition and structure of the materials were obtained via an X-ray diffraction technique, using the PANalytical Empyrean (Almelo, The Netherlands) equipment provided, with a characteristic Cu X-ray tube (λ CuKα1 = 1.541874 Å). The samples were scanned in air, at room temperature, with a scan increment of 0.02° and a time of 100 s/step in the 2θ angle range of 10–80°. The XRD patterns were indexed using HighScorePlus 3.0.e software and graphically represented using OriginLab 9.0 software.

Scanning electron microscopy was conducted with an FEI Quanta 250 high-resolution microscope and an energy-dispersive X-ray spectrometer from EDAX Ametek (Mahwah, NJ, USA). The spectrometer included an Element Silicon Drift Detector and a Team 4.5 EDS Analysis System. To increase the sample's conductivity, a small layer of gold was applied to it beforehand.

Micromeritics® TriStar II Plus (Norcross-Atlanta, GA, USA) is a fully automated surface area and porosity analyzer that provides rapid, high-throughput analysis with high accuracy. The three-station device improves the speed and efficiency of typical quality control analyses while also providing the accuracy, resolution, and data reduction capabilities required for research. The instrument combines versatility in analysis methodologies and data reduction to enable analyses that are tailored to specific application requirements. The program for data collecting and calculation is known as TriStar II Plus.

Fourier transform infrared spectroscopy (FT-IR) analysis was performed using an ABB MB 3000 FT-IR spectrometer (ABB Inc., Québec, QC, Canada) and the EasiDiff device (PIKE Technologies, Inc., Madison, WI, USA) for powder measurement. The solid composite sample (1% weight) was combined with KBr. For data capture, 64 scans were performed at a resolution of 4 cm^{-1} betweoen 550 and 4000 cm^{-1}. All spectra were measured in transmittance mode. The Horizon MBTM FTIR software version 3.4.0.3 (ABB Inc., Québec, QC, Canada) was used to process the experimental data.

The thermal behavior of ZrO_2-LSGYN samples under nonisothermal conditions was investigated by differential scanning calorimetry (DSC) and thermogravimetry (TG) using SETSYS Evolution 17 (Setaram, Caluire-et-Cuire, France) equipment. The heat flow was calibrated and adjusted at different temperatures using certified materials at 3 heating rates. The samples were heated in alumina crucibles, in a temperature range from 25 to 1200 °C, under a constant flow of pure argon (16 mL/min), and a 10 K min^{-1} heating rate.

Thermal conductivity, thermal diffusivity, and volumetric specific heat were measured at room temperature via transient plane source using the Hot Disk method (TPS 2200, Hot Disk, Göteborg, Sweden) to pairs of cylindrical samples (11 mm diameter and 6 mm height) that were heat-treated at 1500 °C. Briefly, a 2 mm diameter Hot Disk Kapton sensor (code 7577) sandwiched between the two cylindrical replicate samples was used to simultaneously generate heat and monitor the temperature changes. The method directly measured thermal conductivity using a calculation algorithm, produced by the manufacturer, as the instrument's data processing software (HotDiskTPS7.4).

4. Conclusions

Rare earth-doped ZrO_2, characterized by its cubic phase and exceptional properties, like low thermal conductivity, heat capacity, and diffusivity, presents a promising avenue for the development of highly effective anticorrosion coatings.

ZrO_2 doped with rare earth elements (La, Sm, Gd, Yb, Nd) at 1500 °C only exhibits a cubic phase. It is known that the stability of this phase mitigates the danger of phase changes that may undermine the material efficacy. Rare earth doping elements significantly enhance the chemical stability of ZrO_2, making it a more resilient material against corrosive environments. This strategic modification equips ZrO_2 with the ability to withstand aggressive chemicals and conditions, ensuring its longevity and effectiveness as a protective coating. Moreover, this type of ceramic material consistently exhibits remarkable mechanical properties, including exceptional durability and abrasion resistance. These combined attributes position rare earth-doped ZrO_2 as a premier choice for applications demanding robust and enduring corrosion protection.

The elevated concentration of oxygen vacancies and substitutional defects resulting from the augmented doping level significantly enhanced phonon scattering and reduced thermal conductivity. Rare earth-doped ZrO_2 with low thermal conductivity offers a valuable solution for corrosion protection in environments characterized by extreme temperatures.

Our material presents low diffusivity, which is important because it acts as a barrier, limiting the ability of corrosive substances to penetrate the coating and reach the substrate. The low heat capacity values of ZrO_2_LSGYN are beneficial because it means that the material absorbs less heat, which can prevent rapid temperature fluctuations and the associated stresses.

This innovative material offers a unique combination of attributes that address the critical challenges associated with high-temperature corrosion, a pervasive issue that impacts various industries.

Research is in progress to enable the use of synthesized ZrO_2-Ln_2O_3 powders to obtain and characterize ceramic coatings.

Author Contributions: Conceptualization: M.P. and C.F.C.; methodology: C.F.C. and R.R.P.; validation: M.P. and F.G.I.; investigation: A.I.N., A.C.M., I.A.T., M.A.I. and Ș.C.; data curation: M.P., C.F.C. and R.R.P.; writing—original draft preparation: M.P., C.F.C. and F.G.I.; writing—review and editing: R.R.P., C.F.C. and F.G.I.; project administration: C.F.C.; funding acquisition: C.F.C. and M.P. All authors have read and agreed to the published version of the manuscript.

Funding: This work was supported by the Nucleu Program within the National Research Development and Innovation Plan 2022–2027, financed by Ministry of Research, Innovation and Digitization in the frame of contract no. 5N/2023 (Project: PN 23 25 01 01).

Data Availability Statement: The original contributions presented in the study are included in the article, further inquiries can be directed to the corresponding author.

Conflicts of Interest: The authors declare no conflict of interest.

References

1. Zhang, J.; Guo, X.; Jung, Y.G.; Li, L.; Knapp, J. Lanthanum Zirconate Based Thermal Barrier Coatings: A Review. *Surf. Coat. Technol.* **2017**, *323*, 18–29. [CrossRef]
2. Gorelov, V.P. High-Temperature Phase Transitions in ZrO_2. *Phys. Solid State* **2019**, *61*, 1288–1293. [CrossRef]
3. Graeve, O.A. Zirconia. In *Ceramic and Glass Materials*; Springer: New York, NY, USA, 2008.
4. Tolborg, K.; Walsh, A. Exploring the High-Temperature Stabilization of Cubic Zirconia from Anharmonic Lattice Dynamics. *Cryst. Growth Des.* **2023**, *23*, 3314–3319. [CrossRef]
5. Pyda, W.; Haberko, K.; Zurek, Z. Zirconia Stabilized Earth Oxides with a Mixture of the Rare. *J. Eur. Ceram. Soc.* **1992**, *10*, 453–459. [CrossRef]
6. Vassen, R.; Cao, X.; Tietz, F.; Basu, D.; Stöver, D. Zirconates as New Materials for Thermal Barrier Coatings. *J. Am. Ceram. Soc.* **2000**, *83*, 2023–2028. [CrossRef]
7. Liu, D.; Shi, B.; Geng, L.; Wang, Y.; Xu, B.; Chen, Y. High-Entropy Rare-Earth Zirconate Ceramics with Low Thermal Conductivity for Advanced Thermal-Barrier Coatings. *J. Adv. Ceram.* **2022**, *11*, 961–973. [CrossRef]
8. Xu, L.; Wang, H.; Su, L.; Lu, D.; Peng, K.; Gao, H. A New Class of High-Entropy Fluorite Oxides with Tunable Expansion Coefficients, Low Thermal Conductivity and Exceptional Sintering Resistance. *J. Eur. Ceram. Soc.* **2021**, *41*, 6670–6676. [CrossRef]
9. Zhao, P.; Zheng, H.; Li, G.; Geng, Y.; Xiao, Y.; Guo, H.; Peng, P. CMAS Corrosion Resistant of La^{3+}-Yb^{3+}-Ce^{4+} Co-Doped ZrO_2 Based TBCs: Experimental and Theoretical Research. *Ceram. Int.* **2023**, *49*, 19402–19411. [CrossRef]

10. Colbea, C.; Avram, D.; Cojocaru, B.; Negrea, R.; Ghica, C.; Kessler, V.G.; Seisenbaeva, G.A.; Parvulescu, V.; Tiseanu, C. Full Tetragonal Phase Stabilization in ZrO_2 Nanoparticles Using Wet Impregnation: Interplay of Host Structure, Dopant Concentration and Sensitivity of Characterization Technique. *Nanomaterials* **2018**, *8*, 988. [CrossRef]
11. Whyman, G.; Kalashnikov, A.; Zinigrad, M. On the Dependence of the Ionic Conductivity on Dopant Concentration in the Cubic Zirconium Oxide Doped with Oxides of Trivalent Metals. *Solid State Ion.* **2018**, *316*, 34–37. [CrossRef]
12. Wang, Y.L.; Xiong, X. Phase Stability and Thermal Conductivity of La_2O_3, Y_2O_3 stabilized ZrO_2 ceramic for Thermal Barrier Coating Application. In *Advanced Materials Research*; Trans Tech Publications Ltd.: Bäch, Switzerland, 2014; Volume 1033–1034, pp. 907–911.
13. Sasikumar, K.; Bharathikannan, R.; Raja, M.; Mohanbabu, B. Fabrication and Characterization of Rare Earth (Ce, Gd, and Y) Doped ZrO_2 Based Metal-Insulator-Semiconductor (MIS) Type Schottky Barrier Diodes. *Superlattices Microstruct.* **2020**, *139*, 106424. [CrossRef]
14. Loong, C.-K.; Thiyagarajan, P.; Richardson, J.W.; Ozawa, M.; Suzuki, S. Microstructural Evolution of Zirconia Nanoparticles Caused by Rare-Earth Modification and Heat Treatment. *J. Catal.* **1997**, *171*, 498–505. [CrossRef]
15. Park, M.-s.; Kim, B.; Kim, T.; Hong, E.; Lee, H. Phase Formation and Lattice Distortion of Lu_2O_3-Doped ZrO_2 in Comparison with Y_2O_3-Doped ZrO_2. *Int. J. Appl. Ceram. Technol.* **2020**, *17*, 1224–1230. [CrossRef]
16. Jeong, J.; Han, Y.; Sohn, H. Effect of La Doping on Dielectric Constant and Tetragonality of ZrO_2 Thin Films Deposited by Atomic Layer Deposition. *J. Alloys Compd.* **2022**, *927*, 166961. [CrossRef]
17. Madhusudhana, H.C.; Shobhadevi, S.N.; Nagabhushana, B.M.; Krishna, R.H.; Murugendrappa, M.V.; Nagabhushana, H. Structural Characterization and Dielectric Studies of Gd Doped ZrO_2 Nano Crystals Synthesized by Solution Combustion Method. *Mater. Today Proc.* **2018**, *5*, 21195–21204. [CrossRef]
18. Zinatloo-Ajabshir, S.; Salavati-Niasari, M. Facile Route to Synthesize Zirconium Dioxide (ZrO_2) Nanostructures: Structural, Optical and Photocatalytic Studies. *J. Mol. Liq.* **2016**, *216*, 545–551. [CrossRef]
19. Motoc, A.M.; Valsan, S.; Slobozeanu, A.E.; Corban, M.; Valerini, D.; Prakasam, M.; Botan, M.; Dragut, V.; Vasile, B.S.; Surdu, A.V.; et al. Design, Fabrication, and Characterization of New Materials Based on Zirconia Doped with Mixed Rare Earth Oxides: Review and First Experimental Results. *Metals* **2020**, *10*, 746. [CrossRef]
20. Li, Q.; Liu, L.; Wang, Z.; Wang, X. Continuous Hydrothermal Flow Synthesis and Characterization of ZrO_2 Nanoparticles Doped with CeO_2 in Supercritical Water. *Nanomaterials* **2022**, *12*, 668. [CrossRef]
21. Costa, C.Z.; Sousa-Aguiar, E.F.; Couto, M.A.P.G.; Filho, J.F.S.d.C. Hydrothermal Treatment of Vegetable Oils and Fats Aiming at Yielding Hydrocarbons: A Review. *Catalysts* **2020**, *10*, 843. [CrossRef]
22. Koch, C.C. *Nanostructured Materials: Processing, Properties and Potential Applications*; Noyes Pub.: Hartford, WI, USA; William Andrew Pub.: Hartford, WI, USA, 2002; ISBN 0815514514.
23. Yang, G.; Park, S.J. Conventional and Microwave Hydrothermal Synthesis and Application of Functional Materials: A Review. *Materials* **2019**, *12*, 1177. [CrossRef]
24. *ASTM E1479-24*; Standard Practice for Describing and Specifying Inductively Coupled Plasma Atomic Emission Spectrometers. ASTM International: West Conshohocken, PA, USA, 2024.
25. Terki, R.; Bertrand, G.; Aourag, H.; Coddet, C. Structural and Electronic Properties of Zirconia Phases: A FP-LAPW Investigations. *Mater. Sci. Semicond. Process.* **2006**, *9*, 1006–1013. [CrossRef]
26. Holder, C.F.; Schaak, R.E. Tutorial on Powder X-ray Diffraction for Characterizing Nanoscale Materials. *ACS Nano* **2019**, *13*, 7359–7365. [CrossRef]
27. Sing, K.S.W.; Everett, D.H.; Haul, R.A.W.; Moscou, L.; Pierotti, R.A.; Rouquerol, J.; Siemieniewska, T. Reporting Physisorption Data for Gas/Solid Systems with Special Reference to the Determination of Surface Area and Porosity (Recommendations 1984). *Pure Appl. Chem.* **1985**, *57*, 603–619. [CrossRef]
28. Pandey, M.; Singh, M.; Wasnik, K.; Gupta, S.; Patra, S.; Gupta, P.S.; Pareek, D.; Chaitanya, N.S.N.; Maity, S.; Reddy, A.B.M.; et al. Targeted and Enhanced Antimicrobial Inhibition of Mesoporous ZnO-Ag_2O/Ag, ZnO-CuO, and ZnO-SnO_2 Composite Nanoparticles. *ACS Omega* **2021**, *6*, 31615–31631. [CrossRef]
29. Saikumari, N.; Dev, S.M.; Dev, S.A. Effect of Calcination Temperature on the Properties and Applications of Bio Extract Mediated Titania Nano Particles. *Sci. Rep.* **2021**, *11*, 1734. [CrossRef]
30. Chevalier, J.; Gremillard, L.; Virkar, A.V.; Clarke, D.R. The Tetragonal-Monoclinic Transformation in Zirconia: Lessons Learned and Future Trends. *J. Am. Ceram. Soc.* **2009**, *92*, 1901–1920. [CrossRef]
31. Gupta, T.K.; Bechtold, J.H.; Cadoff, L.H.; Rossing, B.R. Stabilization of Tetragonal Phase in Polycrystalline Zirconia. *J. Mater. Sci.* **1977**, *12*, 2421–2426. [CrossRef]
32. Pérez-Maqueda, L.A.; Matijevi'c, E.M. Preparation and Characterization of Nanosized Zirconium (Hydrous) Oxide Particles. *J. Mater. Res.* **1997**, *12*, 3286–3292. [CrossRef]
33. Guo, G.Y.; Chen, Y.L.; Ying, W.J. Thermal, Spectroscopic and X-ray Diffractional Analyses of Zirconium Hydroxides Precipitated at Low PH Values. *Mater. Chem. Phys.* **2004**, *84*, 308–314. [CrossRef]
34. Dwivedi, R.; Maurya, A.; Verma, A.; Prasad, R.; Bartwal, K.S. Microwave Assisted Sol-Gel Synthesis of Tetragonal Zirconia Nanoparticles. *J. Alloys Compd.* **2011**, *509*, 6848–6851. [CrossRef]
35. Rashad, M.M.; Baioumy, H.M. Effect of Thermal Treatment on the Crystal Structure and Morphology of Zirconia Nanopowders Produced by Three Different Routes. *J. Mater. Process. Technol.* **2008**, *195*, 178–185. [CrossRef]

36. Horti, N.C.; Kamatagi, M.D.; Nataraj, S.K.; Wari, M.N.; Inamdar, S.R. Structural and Optical Properties of Zirconium Oxide (ZrO_2) Nanoparticles: Effect of Calcination Temperature. *Nano Express* **2020**, *1*, 010022. [CrossRef]
37. Pan, Y.; Zhang, J.; Xu, Y.; Gao, Y.; Chen, Z.; Wang, J. A Facile One-Pot Hydrothermal Process to Synthesize Sulfonated Mesoporous ZrO_2. *J. Porous Mater.* **2016**, *23*, 489–495. [CrossRef]
38. Boratto, M.H. Semiconducting and Insulating Oxides Applied to Electronic Devices. Ph.D. Thesis, Incheon National University, Incheon, Republic of Korea, 2018. [CrossRef]
39. Shi, Q.; Yuan, W.; Chao, X.; Zhu, Z. Phase Stability, Thermal Conductivity and Crystal Growth Behavior of RE_2O_3 (RE = La,Yb,Ce,Gd) Co-Doped Y_2O_3 Stabilized ZrO_2 Powder. *J. Solgel. Sci. Technol.* **2017**, *84*, 341–348. [CrossRef]
40. Sun, L.; Guo, H.; Peng, H.; Gong, S.; Xu, H. Influence of Partial Substitution of Sc_2O_3 with Gd_2O_3 on the Phase Stability and Thermal Conductivity of Sc_2O_3-Doped ZrO_2. *Ceram. Int.* **2013**, *39*, 3447–3451. [CrossRef]
41. ZHOU, H.; YI, D. Effect of Rare Earth Doping on Thermo-Physical Properties of Lanthanum Zirconate Ceramic for Thermal Barrier Coatings. *J. Rare Earths* **2008**, *26*, 770–774. [CrossRef]
42. Piticescu, R.R.; Slobozeanu, A.E.; Valsan, S.N.; Ciobota, C.F.; Ghita, A.N.; Motoc, A.M.; Chiriac, S.; Prakasam, M. Hydrothermal Synthesis of Nanocrystalline ZrO_2-$8Y_2O_3$-XLn_2O_3 Powders (Ln = La, Gd, Nd, Sm): Crystalline Structure, Thermal and Dielectric Properties. *Materials* **2021**, *14*, 7432. [CrossRef]
43. Available online: https://www.morgantechnicalceramics.com/en-Gb/Materials/Zirconia-ZrO2/ (accessed on 20 September 2024).
44. Pasupuleti, K.T.; Ghosh, S.; Ramaswamy, P.; Narayana Murty, S.V.S. Zirconia Based Pyrochlore Thermal Barrier Coatings. In *IOP Conference Series: Materials Science and Engineering*; IOP Publishing Ltd.: Bristol, UK, 9 December 2019; Volume 577.
45. *ASTM E1479-16*; Standard Practice for Describing and Specifying Inductively Coupled Plasma Atomic Emission Spectrometers. ASTM International: West Conshohocken, PA, USA, 2016.